J. Fluid Mech. (1991), *vol.* 228, *pp.* 465–485
Printed in Great Britain

Self-excited compressible flow in a pipe–collar nozzle

By W. C. SELEROWICZ[1], A. P. SZUMOWSKI[1] AND G. E. A. MEIER[2]

[1] Technical University, ul. Nowowiejska 24, 00–665 Warszawa, Poland

[2] Max-Planck-Institut für Strömungsforschung, Bunsenstraße 10, 3400 Göttingen, Germany

(Received 22 January 1990 and in revised form 19 December 1990)

The turbulent flow in a duct with an abrupt increase in its cross-sectional area is very unstable and exhibits strong oscillations. Such a flow is investigated experimentally using a simple device – a pipe–collar nozzle, composed of a convergent nozzle and a pipe lengthened by a collar with an enlarged cross-section. The oscillating flow characteristics are considered over a wide range of flow velocities including both subsonic and transonic flow regimes. Two modes of symmetric and one of asymmetric oscillations are distinguished. For the first mode of symmetric oscillation the jet is separated in each phase of the oscillation cycle, whereas for the second the jet alternately separates and reattaches to the collar wall. Both modes of symmetric oscillations are controlled by shear-layer instability of the collar flow. For low velocities and short collars the oscillation is also affected by the organ-pipe resonance in the preceding pipe. The asymmetric oscillation appears at relatively large flow Mach numbers. This mode exhibits a radial resonance of the jet.

1. Introduction

An abrupt increase in a duct's cross-section usually exists in various kinds of supersonic diffusers, ejector systems, pressure-reducing valves and exhaust valves of internal combustion engines. Self-excited oscillations of large amplitudes occur frequently in such configurations.

The flow always separates at the edge of the intake duct which has a smaller diameter. However, further downstream it reattaches to the wall of the enlarged part at the cross-section when this part is sufficiently long. Otherwise the flow is fully separated, at least for some oscillation phases. In considering this behaviour two configurations can be distinguished: a duct with a long enlarged part and a duct with a short enlarged part.

Most investigations performed hitherto have been focused on the sonic flow from a converging nozzle which was extended with a relatively long duct with an enlarged cross-section (Jungowski 1969; Grabitz 1976; Anderson *et al.* 1977, 1978; Meier *et al.* 1978; Szumowski & Meier 1978). Some types of self-excited oscillations were found in this flow. They appear as regular periodic changes of the reattachment point position involving changes of the separation-region volume and the shock wave pattern.

This paper deals with the flow in a duct with a short part having an enlarged cross-section. Hill & Greene (1977) named this configuration a 'whistler-nozzle' because of its acoustic effect. They recorded a strong influence of internal flow oscillations on the free jet characteristics: an increased mixing rate of the jet with the surrounding air and a faster decay of centreline velocity due to the high turbulence of the oscillating flow. This flow behaviour was also confirmed by Hasan & Hussain (1979, 1982).

The oscillation mechanism has not been comprehensively elucidated in the papers known to the authors. Hill & Greene suggest that the oscillations in this configuration appear as effects of cyclic separation and reattachment in the outlet lip region synchronized by an organ-pipe resonant frequency. Hussain & Hasan (1983) view the whistler-nozzle phenomenon as a coupling of two independent resonance mechanisms: the shear-layer tone resulting from the impingement of the pipe-exit shear layer on the collar lip, and organ-pipe resonance of the pipe nozzle. They come to this view by comparing the flow oscillation characteristics of three configurations: a whistler nozzle, a pipe–ring and a pipe–hole. The shear-layer tone is an important component of a feedback loop for the pipe–ring and pipe–hole cases, but it seems to be a second-order factor for the whistler-nozzle (called hereafter a pipe–collar nozzle) configuration. In the last case the shear-layer instability of a jet confined in the collar appears to be the crucial factor of the oscillation mechanism as suggested by Hill & Greene.

In the experimental investigations cited above, only low flow velocities (up to 60 m/s) were considered. In this case the compressibility of the gas affects the oscillating flow characteristics only very weakly. However, the preliminary investigations performed by Szumowski, Selerowicz & Meier (1985) indicated that the self-excited oscillations also occur for large flow velocities (including the transonic flow range), where compressibility effects become significant. They observed that the oscillating flow features, e.g. frequency, amplitude and flow pattern, vary considerably when the flow Mach number M and the relative collar length L_c/d (d is the pipe diameter) increase. Following this observation, the present work is intended to investigate the oscillating flow characteristics and to elucidate the oscillation mechanisms for a wide range of flow velocities. Only pipe–collar nozzles with relatively short collars are considered.

2. Apparatus and experimental procedure

Figure 1 shows the pipe–collar nozzle configuration used in most of the experiments described below. It is composed of a convergent nozzle which is extended by a constant-cross-section pipe ($d = 12$ mm, $L_p = 60$ mm) and a slideable collar (diameter $D = 18$ mm) forming a sudden cross-section enlargement with step $h = 3$ mm. The pipe–collar nozzle was supplied with compressed air at a total pressure p_0 up to 2.4 bar, which allows subsonic and transonic flow velocities to be achieved.

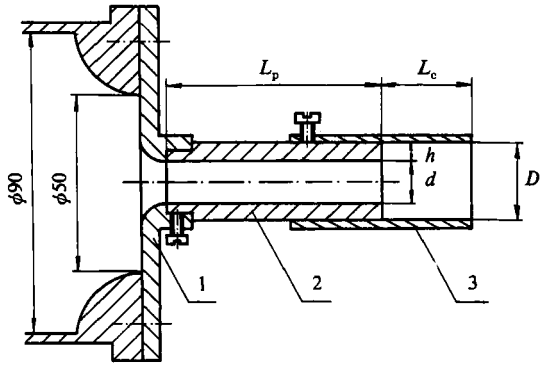

FIGURE 1. Pipe–collar nozzle: $d = 12$ mm, $D = 18$ mm, $h = 3$ mm, $L_p = 60$ mm. 1, Converging nozzle; 2, pipe; 3, collar.

The flow characteristics in the geometry considered were investigated by measuring the flow velocities, the wall pressures and sound pressure levels. The free and confined parts of the jet were visualized to observe flow pattern variations. Miniature piezoresistive Kulite transducers were used for pressure measurements. The signals from the transducers located at various cross-sections along the collar wall were correlated with the base pressure signal (from a transducer located at the pipe cross-section enlargement) to determine the phase relationship. The fluctuating part of the flow velocity signals was measured by means of a 5 μm hot-wire probe in both the confined and free parts of the jet. The signals were filtered in order to separate the fundamental components. Sound pressure levels were measured in the near field of the jet using $\frac{1}{8}$ in. B&K microphones placed in the collar outlet cross-section plane, 0.3 m from the jet axis.

The visualization was carried out by means of a Mach-Zehnder interferometer. A high-intensity photodiode governed by a stroboscope was used as a light source. The controlled delay of the stroboscope allowed artificial freezing of the observed phase of oscillation. The flow photographs were recorded using a video printer. For the pipe–collar nozzle with a circular cross-section only the free-jet visualization was available and thus was not sufficient to deduce in detail the flow pattern inside the collar. To make this possible a pipe–collar nozzle with rectangular cross-section and glass sidewalls was also prepared.

3. General flow characteristics

The pressure signal measured at the cross-section enlargement – the base pressure signal – appears to be a good guide to the oscillating flow behaviour in the configuration considered. The signal changes rapidly when the oscillation starts. Figure 2 shows the variation of the base pressure oscillation amplitude plotted against the ratio of supply pressure to ambient pressure, p_0/p_a. Four characteristic peaks are seen in this figure. The oscillations corresponding to the peaks are very stable: the spectra of the pressure signals display distinct, discrete harmonics (figure

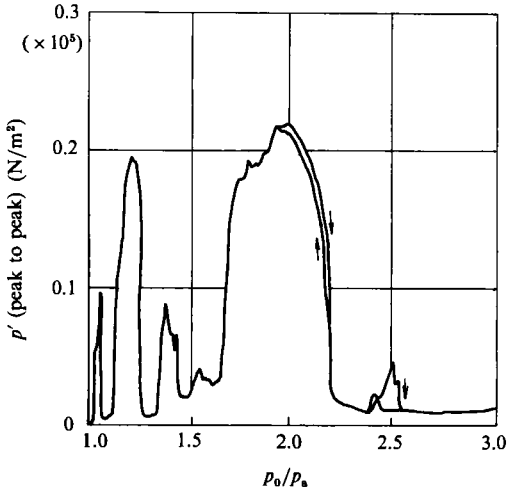

FIGURE 2. Base pressure amplitude variation (peak to peak) with the ratio supply to ambient pressure: L_c = 10 mm. For other dimensions, see figure 1.

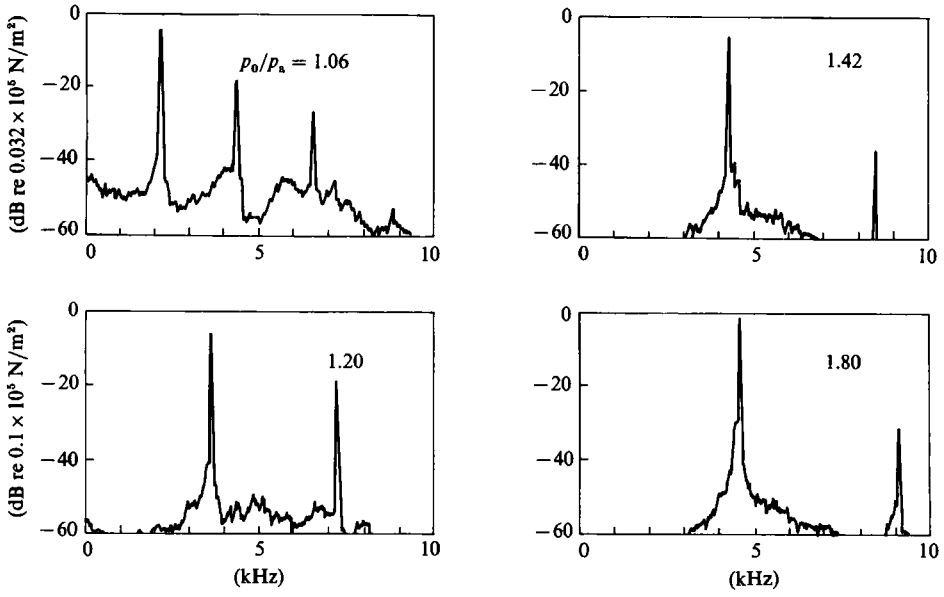

FIGURE 3. Frequency spectra of the base pressure signals for various pressure ratios p_0/p_a: $L_c = 10$ mm.

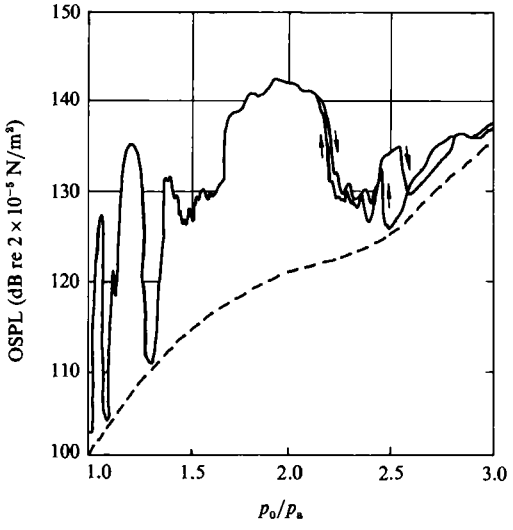

FIGURE 4. Variation of overall sound pressure level with pressure ratio p_0/p_a: — pipe–collar nozzle ($L_c = 10$ mm); - - - pipe nozzle (without collar).

3) of amplitudes 40–50 dB larger than the amplitude of the pressure signals from random distortions.

The appearance of the oscillations is accompanied by a strong increase in the overall sound pressure level (OSPL). Figure 4 shows the OSPL trace corresponding to the base pressure variations plotted in figure 3. As would be expected, the high OSPL values are seen when high base pressure amplitudes occur. An exception occurs in the range $1.5 < p_0/p_a < 1.65$, where the OSPL is relatively high though the base pressure oscillations are weak.

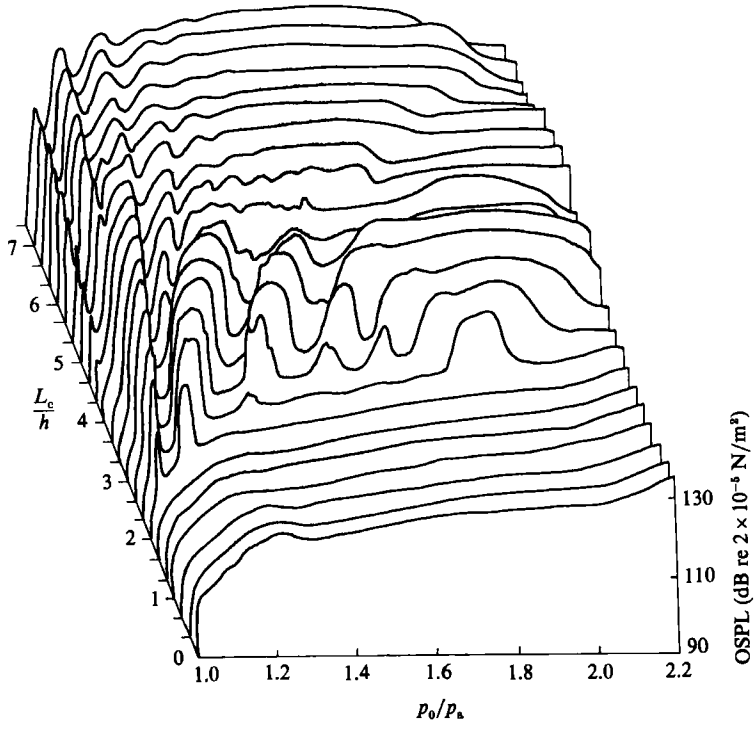

FIGURE 5. Overall sound pressure level versus pressure ratio p_0/p_a for various collar lengths.

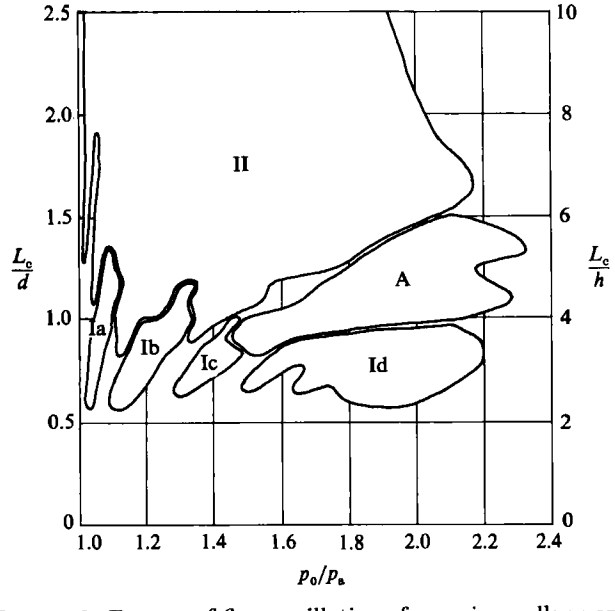

FIGURE 6. Ranges of flow oscillations for a pipe–collar nozzle.

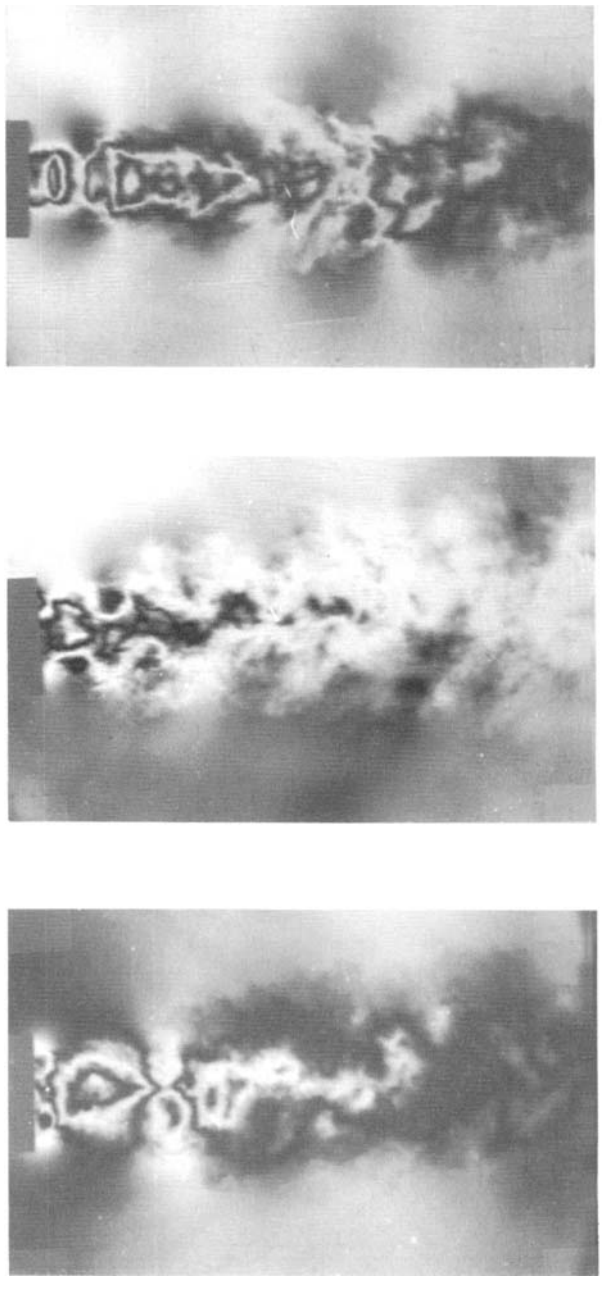

FIGURE 7. Schlieren photographs of an oscillating jet: (*a*) region I, (*b*) region A, (*c*) region II.

Besides the pressure ratio p_0/p_a, the collar length L_c appears to be an important control parameter of the flow considered (Hill & Greene 1977; Hasan & Hussain 1979, 1982; Hussain & Hasan 1983). Figure 5 shows the OSPL traces for collar length changes in steps of 2 mm. The peaks of all traces corresponding to flow oscillations form characteristic ridges in the three-dimensional diagram. This suggests that the flow oscillations displayed by each ridge are of the same type. Following this supposition we have plotted L_c/d against p_0/p_a (figure 6) showing three oscillation

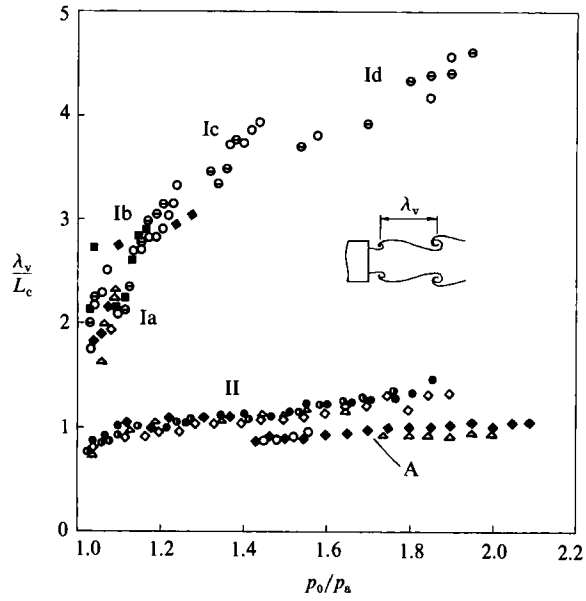

FIGURE 8. Spacing between convected vortices versus pressure ratio p_0/p_a. The collar lengths L_c (mm) are: ■, 8; ⊖, 9; ○, 10; ◆, 12; △, 14; ◇, 16; ●, 20; ◑, 25.

regions: I, II and A (region I is composed of subregions separated by steady flow zones). Regions I and II correspond to symmetric oscillations, whereas region A corresponds to an asymmetric oscillation. This feature can be deduced from interferograms of the free jet presented in figure 7. They show strong toroidal or helical vortices for symmetric and asymmetric oscillations, respectively. The toroidal vortices are convected with a velocity which is approximately equal to $0.6u_j$ (where u_j is the time-averaged centreline flow velocity). An analogous effect was also observed by Ho & Nosseir (1981), who investigated the flow characteristics during jet–plate interaction.

The symmetric oscillations in regions I and II show some different features. This is exhibited in various flow patterns as well as in various amplitude and frequency characteristics. Figure 8 shows the normalized spacing between two succeeding vortices (λ_v/L_c) plotted against the ratio of supply to ambient pressure, p_0/p_a. It is observed that for region II the spacing is nearly independent of p_0/p_a and thereby of the flow velocity. This is not the case for region I, with a ratio λ_v/L_c which clearly increases with increasing p_0/p_a.

The fundamental frequency characteristics for both symmetric oscillations discussed are compared in figure 9. In this figure the Strouhal number ($St_{L_c} = fL_c/u_j$) is plotted versus the flow Mach number M_j for various values of the collar length. Here, both the flow velocity u_j and the flow Mach number M_j are calculated from the isentropic relation for known values of the pressure ratio p_0/p_b (p_b is the time-averaged base pressure) and stagnation temperature of the jet (293 K). For region I (for $L_c = 8$, 10 and 12 mm) the $St_{L_c}(M_j)$ function shows characteristic bands separated by steady flow regions (also see figure 6). In each band St_{L_c} decreases with increasing M_j. Moreover, the locations of the bands along the M_j axis depend on collar length; the bands shift to greater M_j for increasing L_c. These characteristics indicate the effect of the organ-pipe resonance on the phenomenon under consideration

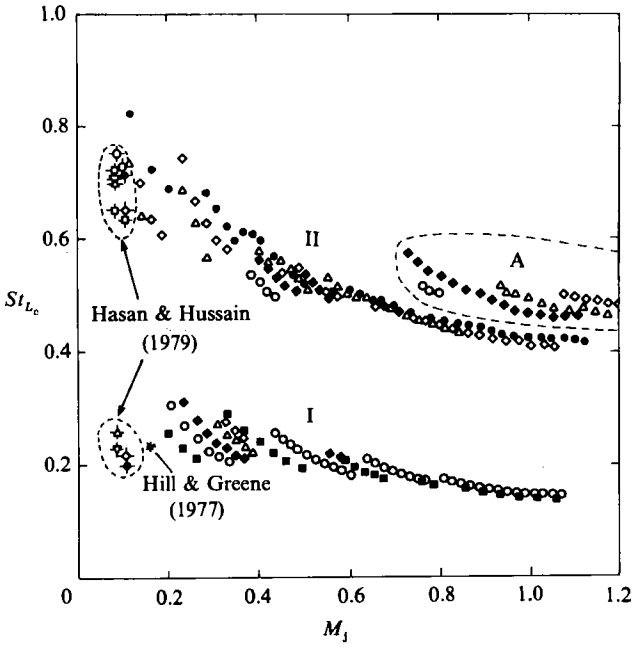

FIGURE 9. Strouhal-number ($St_{L_c} = fL_c/u_j$) variation with flow Mach number M_j. The collar lengths L_c (mm) are: ■, 8; ○, 10; ◆, 12; △, 14; ◇, 16; ●, 20.

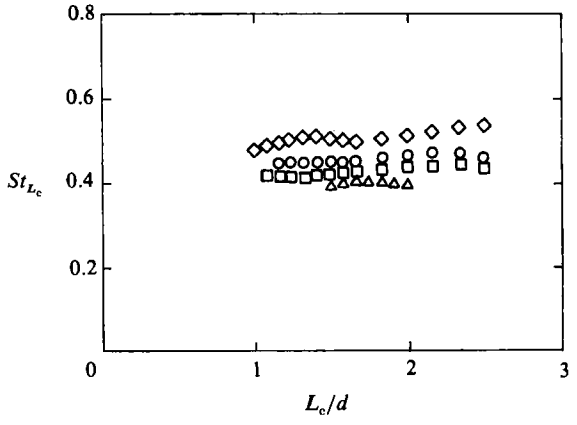

FIGURE 10. Strouhal-number variation with non-dimensional collar length L_c/d. Pressure ratios p_0/p_a are: ◇, 1.20; ○, 1.40; □, 1.60; △, 2.00.

(Hussain & Hasan 1983). This effect, however, weakens with increasing flow Mach number.

In contrast to the case discussed above, the fundamental frequency for region II increases almost monotonically as M_j increases. However, the collar length for the region seems to have negligible influence on the Strouhal number. This observation can be better displayed using the $St_{L_c}(L_c)$ representation shown in figure 10. It is observed that for each velocity considered in this figure the Strouhal number maintains a nearly constant value as the collar length increases. This means that the

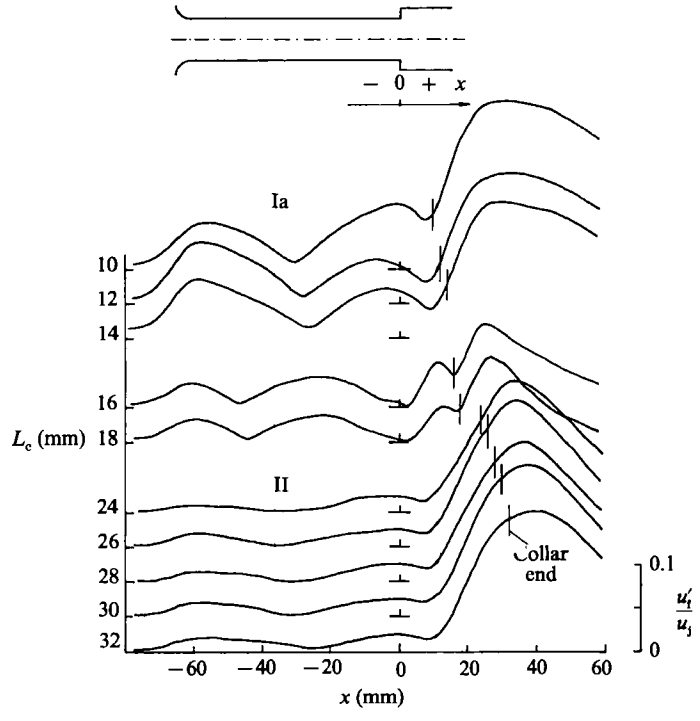

FIGURE 11. Centreline evolution of flow velocity fluctuation amplitude (fundamental) for various collar lengths: $p_0/p_a = 1.05$.

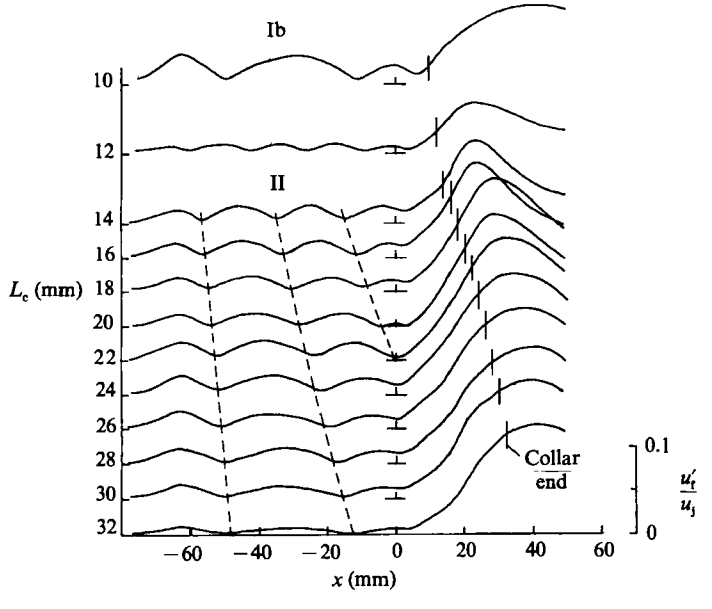

FIGURE 12. Centreline evolution of flow velocity fluctuation amplitude (fundamental) for various collar lengths: $p_0/p_a = 1.20$.

fundamental frequency appears to be inversely proportional to L_c. In this case the organ-pipe resonance is of minor significance. Note that the fundamental frequencies measured by Hussain & Hasan (1983) for low flow velocities correspond to regions I or II, depending on the collar length (figure 9).

The oscillations corresponding to the different regions in the L_c/d, p_0/p_a plane (see figure 6) are characterized by various streamwise distributions of the fundamental amplitude u_f'. This feature is illustrated in figures 11 and 12, in which the distributions of u_f' (normalized by the time-averaged flow velocity u_j) are collected for various collar lengths increasing in steps, and for two values of the pressure ratio $p_0/p_a = 1.05$ and 1.2. These values are chosen to show the evolution of oscillations corresponding to the subregions Ia and Ib, both into oscillations corresponding to region II (see figure 6). The u_f' distributions for a short collar ($L_c = 10$ mm) presented in figures 11 and 12 indicate the organ-pipe resonance for both cases considered: a half-wave mode for the subregion Ia and a full-wave mode for the subregion Ib. The distributions are shown to be maximum at the pipe outlet, which is characteristic for the open end of the pipe. At a value of L_c which corresponds to the bottom boundary of region II the organ-pipe resonance suddenly changes its mode. It transforms into the full-wave mode or the double-wave mode for $p_0/p_a = 1.05$ and 1.20, respectively. This stage, however, called hereafter the intermediate stage, appears for low pressure ratios only. Note that for the intermediate stage for $p_0/p_a = 1.05$ ($L_c = 16$ and 18 mm) the u_f' distribution is at a minimum at the pipe exit. This apparently contradicts the one-dimensional model of organ-pipe resonance. In this case the effective organ-pipe length is clearly greater than the pipe length alone; it includes a part of the jet in the collar (Hasan & Hussain 1979). For $p_0/p_a = 1.20$ the intermediate stage ($L_c = 12$ mm) shows a very weak organ-pipe resonance which is in accordance with the one-dimensional model.

It follows from these characteristics that organ-pipe resonance appears to be a substantial factor controlling the flow oscillations corresponding to both subregions Ia and Ib, as well as to the intermediate stage for low pressure ratios. For region II (beyond the intermediate stage, in figure 11 the curves $L_c = 24$ mm to 32 mm, and in figure 12 the curves $L_c = 14$ to 32 mm) the organ-pipe resonance seems to be a factor of second order in the phenomenon considered. In this case the length of the acoustic wave increases continuously with increasing L_c. Consequently the mode of organ-pipe resonance changes continuously. For $p_0/p_a = 1.20$ it changes from the one-and-a-half-wave mode for $L_c = 14$ mm to a full-wave mode for $L_c = 32$ mm. This is possible owing to the contribution to the resonance phenomenon of the jet confined in the collar. This contribution changes continuously depending on the fundamental frequency. In this case, in contrast to the oscillations corresponding to the subregions Ia and Ib, the organ-pipe resonance has a secondary significance. It confirms the conclusion drawn from the frequency characteristics (see figure 10).

As can be observed in figure 11, organ-pipe resonance affects the fundamental amplitude distribution along the collar. This distribution has a minimum for a half-wave mode (the curves $L_c = 10$, 12 and 14 mm) and a maximum for a full-wave mode (the curves $L_c = 16$ and 18 mm). Hussain & Hasan (1983) interpret the u_f' distribution in the collar as being dependent on the relative contribution of the instability wave and the acoustic wave. The first is induced by the shear-layer instability which is exhibited in toroidal vortices (see figure 7) whereas the second is the harmonic sound wave which issues from the pipe (this wave spreads in the collar space and in the ambient fluid). Hussain & Hasan (1983) assume that the acoustic wave is the effect of the shear-layer impingement on the collar lip. This assumption has not, however,

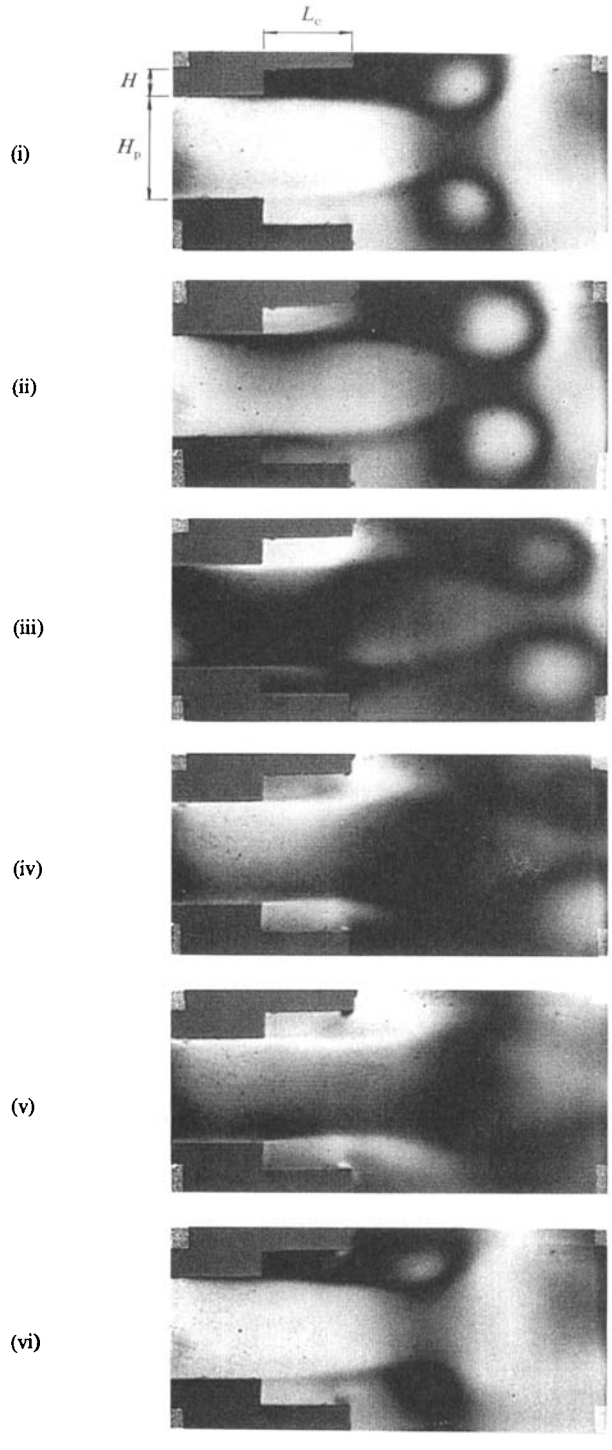

FIGURE 13. Stroboscopic interferograms of oscillating flow in a rectangular nozzle ($L_p = 60$ mm, $L_c = 10$ mm, $H_p = 12$ mm, $H = 3$ mm, $p_0/p_a = 1.05$, $M_j = 0.27$, $f = 1650$ Hz, mode I). The phase, $\phi/2\pi$, values for successive pictures are: (i) 0, (ii) 1/6, (iii) 2/6, (iv) 3/6, (v) 4/6, (vi) 5/6. Flow direction is from left to right.

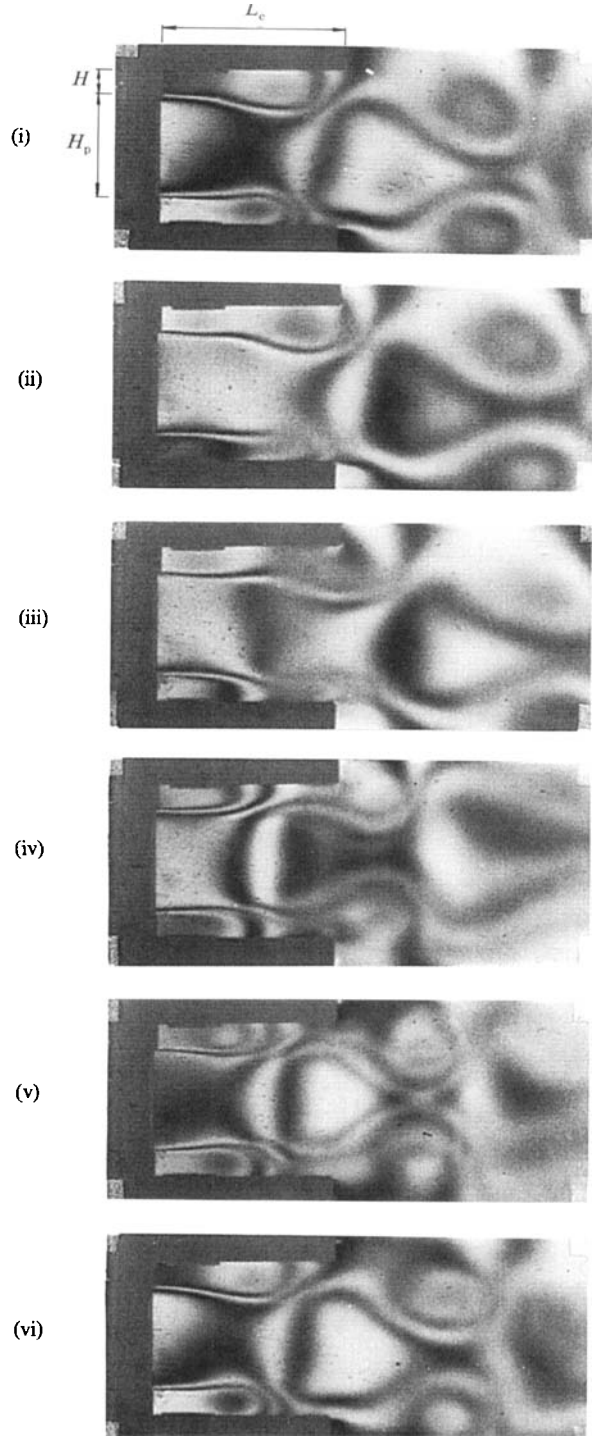

FIGURE 14. Interferograms of oscillating flow in a rectangular nozzle ($L_p = 50$ mm, $L_c = 20$ mm, $H_p = 12$ mm, $H = 3$ mm, $p_0/p_a = 1.24$, $M_j = 0.65$, $f = 4550$ Hz, mode II). Phases, $\phi/2\pi$, for successive pictures are: (i) 0, (ii) 1/6, (iii) 2/6, (iv) 3/6, (v) 4/6, (vi) 5/6. Flow direction is from left to right.

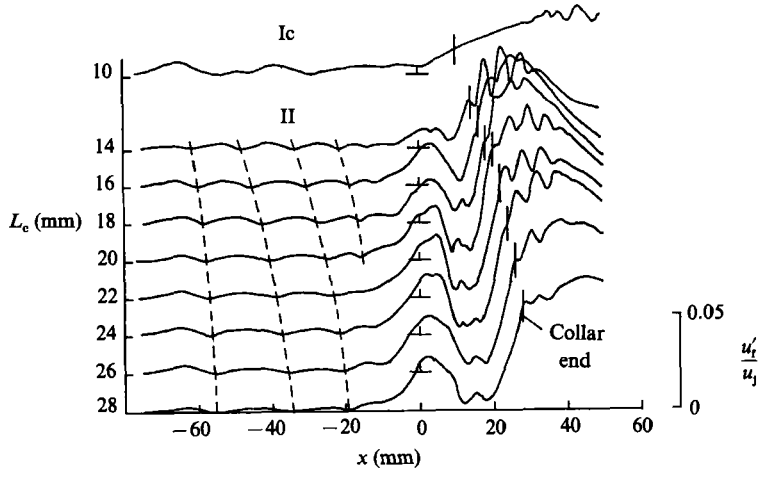

FIGURE 15. Centreline evolution of flow velocity fluctuation amplitude (fundamental) for various collar lengths: $p_0/p_a = 1.40$.

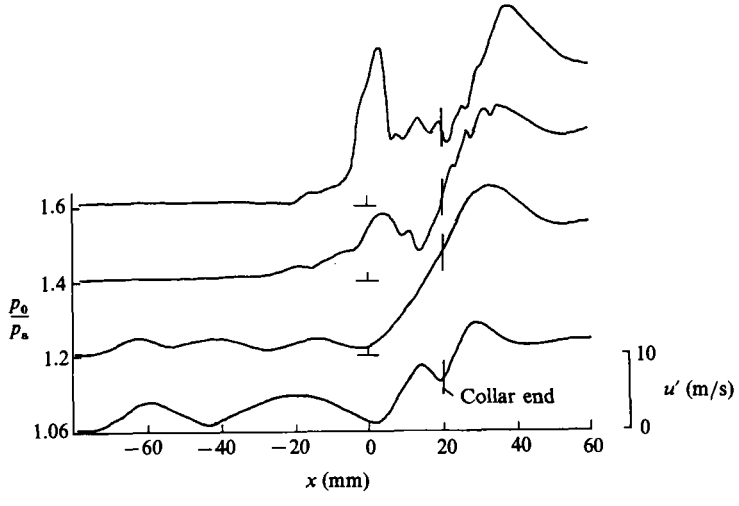

FIGURE 16. Centreline evolution of flow velocity fluctuation amplitude for various values of pressure ratio p_0/p_a.

been confirmed in our experiments. The curves presented in figures 11 and 12 prove that in most cases considered the main contribution to the u'_f variation in the collar is due to the instability wave. This variation is disturbed by the acoustic wave issuing from the pipe, the strength of which is proportional to the amplitude of the organ-pipe resonance. When the amplitude is small, the u'_f variation along the collar maintains a nearly invariant shape as L_c increases (see the curves for $L_c \geqslant 24$ mm in figure 11 and the curves for $L_c \geqslant 12$ mm in figure 12).

The internal flow visualization performed for two-dimensional flow cases yields additional arguments for the conclusions mentioned above. It shows that for subregions Ia (figure 13), Ib, Ic and Id, the jet is separated from the collar wall in each phase of the oscillation cycle, though the jet width (jet diameter in the axisymmetric flow) varies distinctly. On the other hand, the oscillations cor-

responding to region II (figure 14) are characterized by periodically alternating reattachment and separation of the whole jet (not only of its shear layer), as was predicted by Hill & Greene.

The experimental results discussed above show that organ-pipe resonance only plays an important role in the phenomenon considered for relatively small flow Mach numbers (small p_0/p_a) and short collars. For large M_j pipe resonance appears only in a minor role, or disappears altogether. Such cases are shown in figures 15 and 16. Figure 15 the u_f' distributions indicate weak pipe resonance which, however, is strongly disturbed at the outlet part of the pipe owing to the flow instability in the collar. In figure 16 the u_f' distributions for various p_0/p_a values increasing in steps and for constant collar length (corresponding to region II) are presented. Note that the pipe resonance amplitude decreases with increasing p_0/p_a. For the largest pressure ratio ($p_0/p_a = 1.6$) the resonance is not perceptible.

4. Oscillation mechanisms

The flow characteristics described above indicate the following two types of symmetric oscillations: separated flow oscillations (SFO) and separation reattachment oscillations (SRO). The first correspond to region I, and the second to region II in the L_c/d, p_0/p_a plane (see figure 6). The following most probable mechanisms for these oscillations can be proposed.

4.1. *The separated flow oscillations (SFO)*

This oscillation type appears for a relatively short collar. The characteristic flow patterns during the oscillation are displayed schematically in figure 17. The points (i) to (vi) in the base pressure and flow velocity traces presented in figure 18 correlate with these patterns. The phase (i) corresponds to the maximum value of the base pressure signal. The centreline velocity at the pipe outlet cross-section is at its minimum, whereas at the collar exit it is at its maximum (figure 18). Close to this point the air from the 'dead-water region' begins flowing out into the ambient air. Consequently the shear layer in the region near the collar lip moves outwards (ii, iii) causing the jet cross-section to increase in this phase. This increase is accompanied by a decrease in the centreline flow velocity at the collar outlet cross-section (u_B in figure 18). As the base pressure decreases, the air flowing out from the separation bubble is cut off and a backflow emerges. Consequently the shear layer rolls up, causing ring vortex formation (iv). The vortex gains strength. However, it stays in almost the same position owing to the momentum balance between the shear layer and the backflow. This balance is lost at higher values of the flow velocity near the collar outlet cross-section (v). Therefore the vortex leaves the collar (vi). Now, the dead-water region fills quickly with ambient air, and the base pressure increases. This increase is sustained owing to the relatively low gas injection by the jet which has decreased flow velocity at the outlet cross-section (u_A in figure 18). In this phase both decreasing injection and gas insertion affect the base pressure. It achieves a value greater than the ambient pressure. In this way the cycle is repeated.

The crucial role in this mechanism is played by the vortex generation process inside the collar. It is initiated by the shear-layer waving in the vicinity of the outlet cross-section of the pipe and amplified by the backflow of the ambient air. The shear-layer waving is caused by the base pressure oscillations and, for low flow velocities, also by organ-pipe resonance. On the other hand the backflow appears, owing to the gas injection inside the collar. For low flow velocities the gas injection is relatively

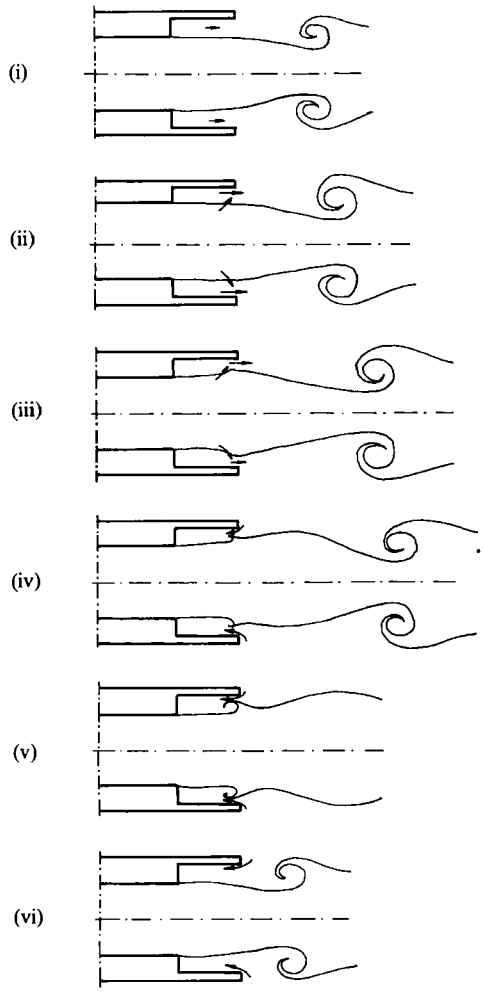

FIGURE 17. Schematized flow patterns for SFO. Phases $\phi/2\pi$, for successive pictures are: (i) 0, (ii) 1/6, (iii) 2/6, (iv) 3/6, (v) 4/6, (vi) 5/6.

weak. In this case the shear-layer waving is the most important factor for the ring vortex formation. The waving is strongest when the base pressure oscillation is synchronized with the organ-pipe resonance. When such a synchronization does not occur the oscillation weakens or disappears. In contrast to the above, for large flow velocities the amplification effect, caused by the gas injection, is so strong that the shear-layer waving can be weak. In this case the base pressure oscillation appears to be sufficient to initiate the vortex formation.

In order to check the effect of organ-pipe resonance in the oscillation mechanism, we have performed some experiments with a collar nozzle configuration where the pipe between the nozzle and the collar was removed. The fundamental frequencies corresponding to this case are marked in figure 19 by filled points. Note that the SFO for the collar nozzle only occur in the transonic flow.

As mentioned above, organ-pipe resonance appears to be an important factor for the oscillating flow under consideration, when the flow Mach number is relatively low. In this case the fundamental frequency appears as the mean value of the natural

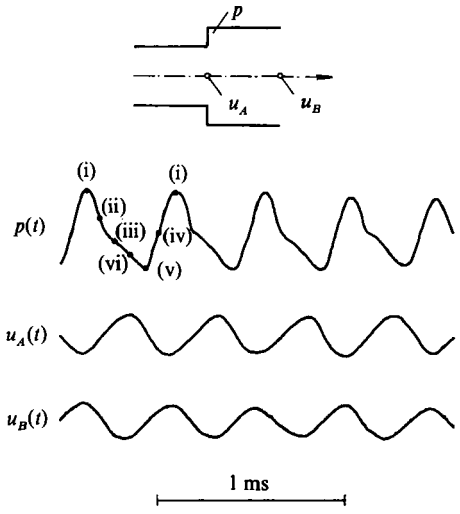

FIGURE 18. Base pressure and velocity traces for SFO: $L_c = 10$ mm, $p_0/p_a = 1.05$, $f = 2150$ Hz. Points (i) to (vi) denote oscillation phases (see figure 17).

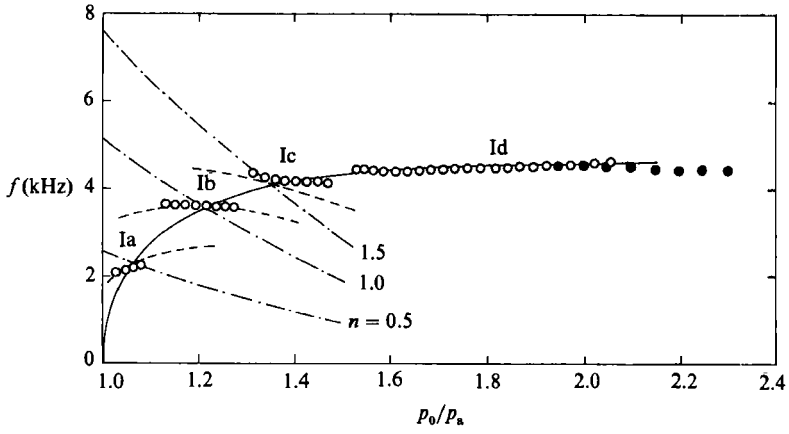

FIGURE 19. Measured (pipe–collar nozzle – open symbols; collar nozzle – filled symbols) and predicted (dashed lines) frequencies for SFO: $L_c = 10$ mm.

generator frequency (the continuous line in figure 19 drawn through the points of maximum excitation of the segments Ia to Id) and the organ-pipe frequency for the half-wave, full-wave and one-and-a-half-wave mode resonator (dashed lines).

It was mentioned above that in some phase of flow oscillation the ambient air is sucked into the collar (figure 17). The flow rate of the sucked air depends above all on the instantaneous value of the ambient and base pressure difference. However, it is also influenced by the shape of the collar lip, which results in a contraction of the backflow stream. Figure 20 shows the OSPL traces versus pressure ratio p_0/p_a for two collar lips: the first has sharp and the second has rounded edges. In the second case the OSPL is distinctly greater, which corresponds to more intensive jet oscillations. It appears because of the greater backflow rate, due to a lower contraction for rounded lip edges.

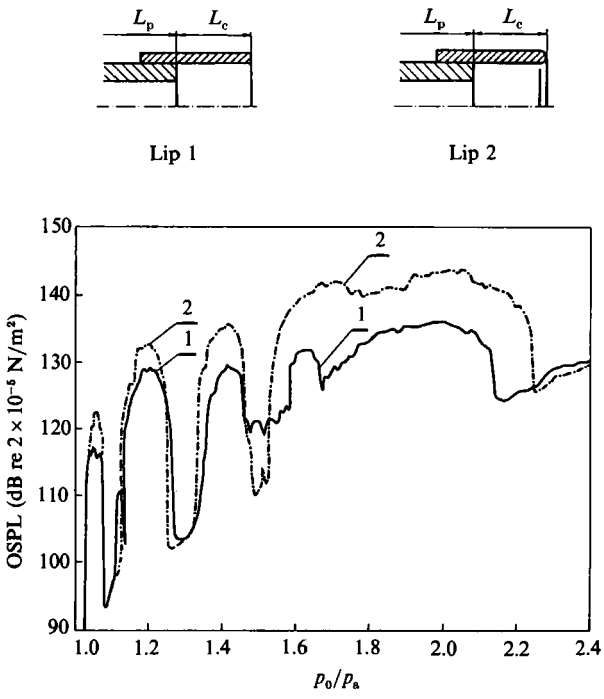

FIGURE 20. Overall sound pressure level variations with pressure ratio p_0/p_a for two forms of collar lip: $L_c = 10$ mm.

4.2. *The separation reattachment oscillations (SRO)*

This oscillation occurs when the collar is relatively long (see figure 6). An interesting characteristic feature of this oscillation is a non-monotonic variation of the wall-pressure signal amplitude, shown in figure 21 (for the SFO, the amplitude decreases slightly along the collar). This variation is independent of the flow velocity under consideration, and shows a deep minimum at approximately $x/h = 3.3$. The phase variation of pressure signals presented in figure 22 shows a high phase velocity in the collar part close to the cross-section enlargement, and a low phase velocity in the remaining part. Both variations displayed in figures 21 and 22 allow the instantaneous pressure distributions along the collar to be drawn as shown in figure 23. These distributions, as well as the flow interferograms in the rectangular duct (figure 14), substantiate the following mechanisms for the SRO (figure 24). Our description starts with the reference phase ($\phi/2\pi = 0$) corresponding to the pressure distribution, the flow interferograms and the schematic flow pattern denoted by (i) in figures 23, 14 and 24, respectively. The following flow characteristics correspond to this phase: the base pressure is maximum, the wall pressure is minimum at $x/h \approx 5$, and a strong vortex which is present inside the collar is convected with the stream. The vortex motion is accompanied in the next phase (ii) by a shift of the low-pressure region (figure 23). In the phase $\phi/2\pi = 0.33$ (iii) the vortex leaves the collar. Now the wall pressure has a minimum value close to the collar lip. Simultaneously a new vortex builds inside the collar. At phase $\phi/2\pi = 0.5$ (iv), the high-pressure region appears at $x/h \approx 5$. The flow interferogram corresponding to this phase indicates flow reattachment at this point. Now there is a minimum base pressure.

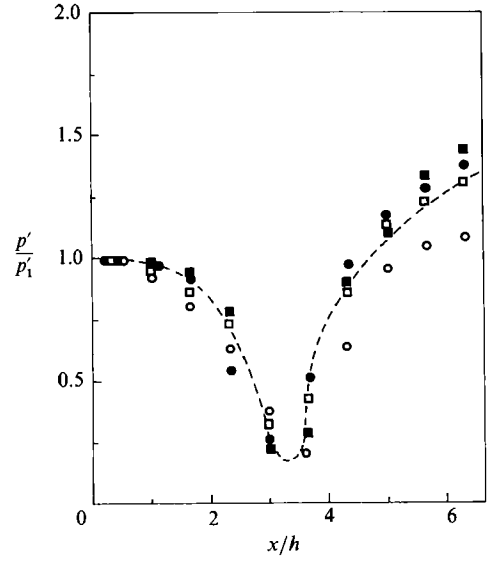

FIGURE 21. Amplitude of wall-pressure signal along the collar for SRO: $L_c = 20$ mm, $L_c/h = 6.67$. Pressure ratio p_0/p_a and oscillation frequency f (Hz) are: ○, 1.20. 4600; ■, 1.40, 5620; □, 1.60, 6220; ●, 1.80, 6620.

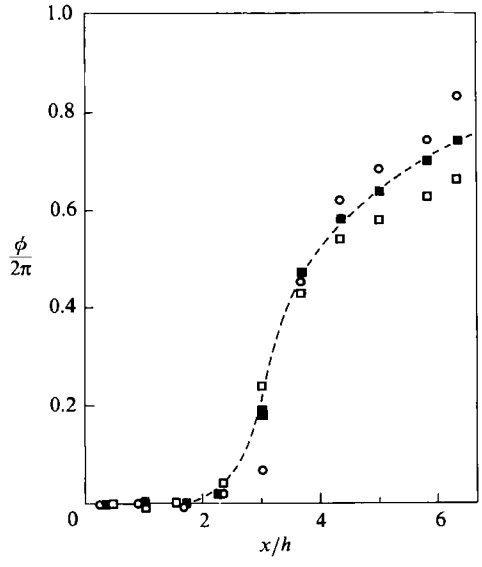

FIGURE 22. Phase variation $\phi/2\pi$ of wall-pressure signals along the collar (see description in figure 21).

Owing to a high positive pressure gradient just upstream from the stagnation point, the separation bubble grows. In effect, the stagnation point shifts downstream, up to the collar lip.

As mentioned in §3 the SRO in the pipe-collar nozzle are also practically unaffected by the organ-pipe resonance for low flow velocities. For the collar nozzle

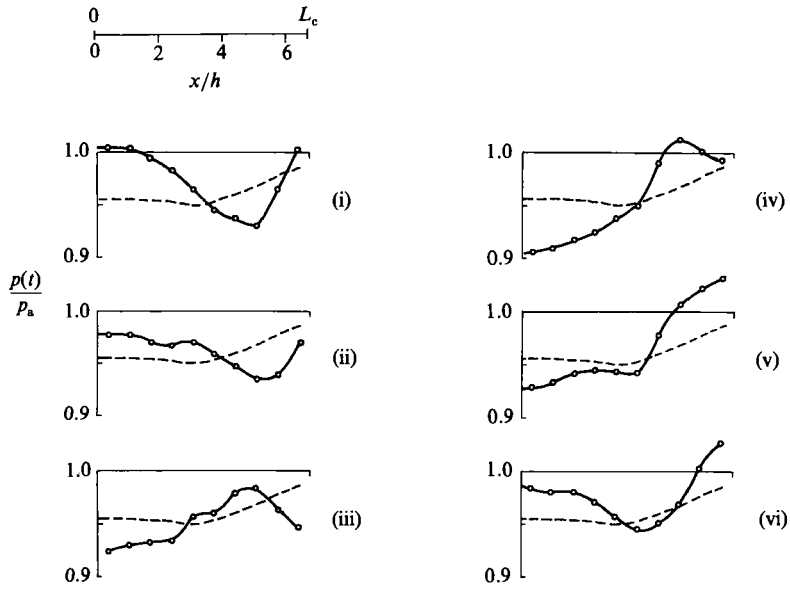

FIGURE 23. Instantaneous wall-pressure distributions along the collar for SRO: $L_c = 20$ mm, $L_c/h = 6.67$, $p_0/p_a = 1.20$, $M_j = 0.54$, $f = 4600$ Hz. Phases $\phi/2\pi$ for successive pictures are: (i) 0, (ii) 1/6, (iii) 2/6, (iv) 3/6, (v) 4/6, (vi) 5/6.

the SRO appears in nearly the same range of p_0/p_a as for the pipe–collar nozzle (figure 25). In both cases the SRO is controlled by the vortex convection inside the collar. Following the SRO mechanism described above, one can predict the oscillation frequency. The period of oscillation T can be divided into two time segments t_1 and t_2. During t_1 the vortex travels a distance L_v from the origin to the collar lip, whereas during the time t_2 the pressure perturbation, which emerges when the vortex leaves the collar, moves upstream (from the collar exit to the vortex origin position). Thus

$$T = L_v(1/u_v + 1/c),$$

where u_v is the vortex convection velocity inside the collar and c denotes the speed of sound. For the collar length $L_c = 20$ mm, L_v was experimentally determined as 13 mm and u_v as $0.37u_j$.

The oscillation frequencies calculated from those data are shown in figure 25 by a continuous line and are compared with the experimental data for the pipe–collar nozzle (open symbols) and the collar nozzle (filled symbols).

4.3. *The asymmetric oscillation*

The asymmetric mode seems to be more difficult to explain. The base pressure measurements show that during this oscillation the base pressure is nearly constant (see the range $1.5 < p_0/p_a < 1.65$ in figure 2). The flow velocity measurements along the centreline, taken inside the collar, do not exhibit any oscillation either. Oscillations were observed beyond the collar exit in the free jet; however, the contribution of the discrete components to the velocity oscillation spectrum was very small. This proves that the helical vortex, displayed in the jet mixing layer, does not influence the jet core. The oscillation can therefore only be detected by means of flow visualization and acoustic measurements. The structure of the helical vortex,

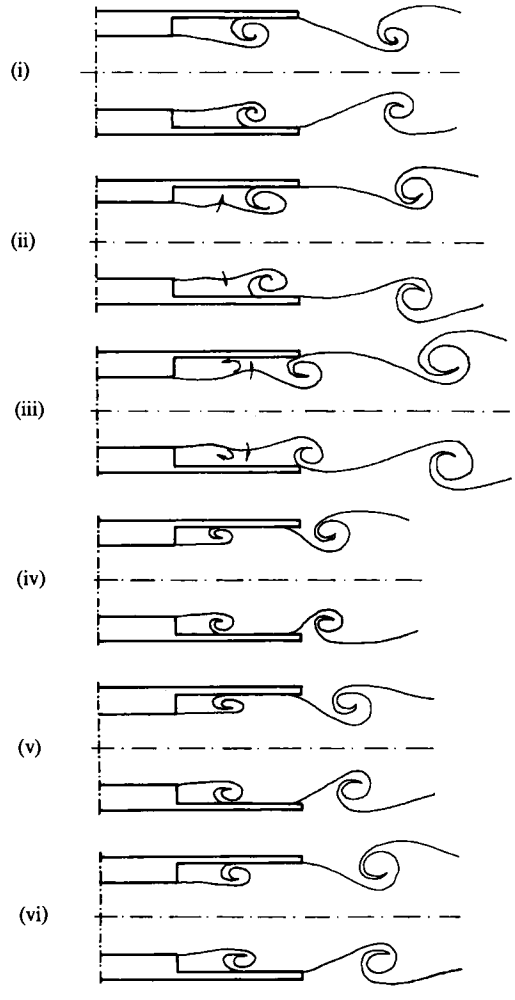

FIGURE 24. Schematized flow patterns for SRO. Phases $\phi/2\pi$ for successive pictures are: (i) 0, (ii) 1/6, (iii) 2/6, (iv) 3/6, (v) 4/6, (vi) 5/6.

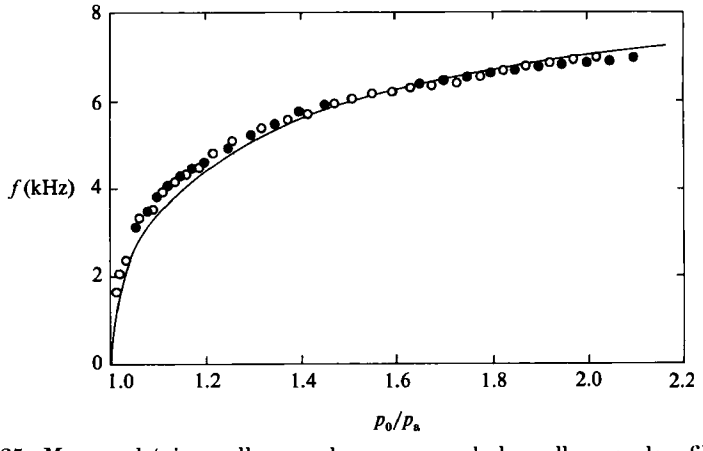

FIGURE 25. Measured (pipe–collar nozzle – open symbols; collar nozzle – filled symbols) and predicted frequencies for SRO: $L_c = 20$ mm.

observed by means of visualization, suggests that the vortex originates at the pipe-exit edge. Pictures of the successive stages show, furthermore, that the starting point moves around the edge with the oscillation frequency. It is possible that this oscillation is controlled by the helical neutral wave mode predicted by Tam & Hu (1989) for high-speed jets.

5. Concluding remarks

The self-excited oscillations of pipe–collar nozzle flow in subsonic and transonic flow regimes exhibit at least three oscillation types: (1) symmetric oscillations, (SFO), where the jet remains separated in each oscillation phase; (2) symmetric oscillations, (SRO), where the dead-water region is separated from the ambient air in each oscillation phase; and (3) asymmetric oscillations characterized by rotating separation.

The SFO are controlled by the shear-layer instability of the jet confined in the collar. For low flow velocity they are also affected by the organ-pipe resonance. The SRO are controlled only by the flow in the collar. Preliminary investigations indicate that for long collars two or more ring vortices occur simultaneously (in the collar). The asymmetric oscillations have been examined only tentatively in this paper, and require detailed investigations which are being continued by the authors.

REFERENCES

ANDERSON, J. S., JUNGOWSKI, W. M., HILLER, W. J. & MEIER, G. E. A. 1977 Flow oscillations in a duct with a rectangular cross-section. *J. Fluid Mech.* **79**, 769–784.

ANDERSON, J. S., JUNGOWSKI, W. M., MEIER, G. E. A. & WITCZAK, K. J. 1978 Self-excited oscillations in a duct flow with oblique shock waves. *Proc. Inst. Acoust.*, vol. 7, pp. 15.M2.1–15.M2.4.

GRABITZ, G. 1976 Überschallströmung in einem Kanal mit plötzlicher Querschnittserweiterung. *MPI f. Strömungsforschung, Göttingen, Bericht* 14/1976.

HASAN, M. A. Z. & HUSSAIN, A. K. M. F. 1979 A formula for resonance frequencies of a whistler-nozzle. *J. Acoust. Soc. Am.* **65**, 1140–1142.

HASAN, M. A. Z. & HUSSAIN, A. K. M. F. 1982 The self-excited axisymmetric jet. *J. Fluid Mech.* **115**, 59–89.

HILL, W. G. & GREENE, P. R. 1977 Increased turbulent jet mixing rates obtained by self-excited acoustic oscillations. *Trans. ASME* I: *J. Fluids Engng* **99**, 520–525.

HO, C.-M. & NOSSEIR, N. S. 1981 Dynamics of an impinging jet. Part 1. The feedback phenomenon. *J. Fluid Mech.* **105**, 119–142.

HUSSAIN, A. K. M. F. & HASAN, M. A. Z. 1983 The 'whistler-nozzle' phenomenon. *J. Fluid Mech.* **134**, 431–458.

JUNGOWSKI, W. M. 1969 On the flow in a sudden enlargement of a duct. *Fluid Dyn. Trans.* **4**, 231–241.

MEIER, G. E. A , GRABITZ, G., JUNGOWSKI, W. M., WITCZAK, K. J. & ANDERSON, J. S. 1978 Oscillations of supersonic flow downstream of an abrupt increase in duct cross-section, *Mitteilungen aus dem MPI f. Strömungsforschung und der AVA Göttingen Bericht* 65/1978.

SZUMOWSKI, A. P. & MEIER, G. E. A. 1978 Schwingungen der Überschallströmung in einem Kanal mit Querschnittsprung. *MPI f. Strömungsforschung, Göttingen, Bericht* 23/1978.

SZUMOWSKI, A. P., SELEROWICZ, W. C. & MEIER, G. E. A. 1985 Oscillations of a subsonic flow in an abruptly expanding circular duct. Lecture Notes in Physics, Vol. 235, pp. 28–40. Springer.

TAM, C. K. W. & HU, F. Q. 1989 On the three families of instability waves of high-speed jets. *J. Fluid Mech.* **201**, 447–483.